



**University of
Sunderland**

Emran, Mohammed Y., Mekawy, Moataz, Akhtar, Naeem, Shenashen, Mohamed A., EL-Sewify, Islam M., Faheem, Ahmed and El-Safty, Sherif (2018) Broccoli-shaped biosensor hierarchy for electrochemical screening of noradrenaline in living cells. *Biosensors and Bioelectronics*, 100. pp. 122-131. ISSN 09565663

Downloaded from: <http://sure.sunderland.ac.uk/id/eprint/8521/>

Usage guidelines

Please refer to the usage guidelines at <http://sure.sunderland.ac.uk/policies.html> or alternatively contact

sure@sunderland.ac.uk.

Broccoli-shaped Biosensor Hierarchy for Electrochemical Screening of Noradrenaline in Living Cells

M.Y. Emran¹, M. Mekawy¹, N. Akhtar¹, M.A. Shenashen¹, I. M. EL-Sewify¹, A. Faheem², S. A. El-Safty^{1,3,*}

¹ National Institute for Materials Science (NIMS), Research Center for Functional Materials, 1-2-1 Sengen, Tsukuba-shi, Ibaraki-ken, 305-0047, Japan.

² School of Pharmacy and Pharmaceutical Sciences, Faculty of Health Sciences and Wellbeing, University of Sunderland, Sunderland, SR1 3SD, UK

³ Graduate School for Science and Engineering, Waseda University, 3-4-1 Okubo, Shinjuku-ku, Tokyo 169-8555, JAPAN.

E-mail: sherif.elsafty@nims.go.jp

Abstract

Monitoring and determination of ultra-trace concentrations of monoamine neurotransmitter such as noradrenaline (NA) in living cells with simple, sensitive and selective assays are significantly interesting. We designed NA-electrode sensing system based on C-, N-doped NiO broccoli-like hierarchy (CNNB). The spherical broccoli-head umbrella architectures associated with abundant nano-tubular arrangements enabled to tailor building, and control surface morphology of biosensor electrodes with tunable, and multi-diffusive open-spaces, holes, windows and caves aligned vertically along the entire trunk axes connected with spherical CNNB heads. The homogenous doping and anisotropic dispersion of CN nanospheres along the entire NB head nanotubes lead to create abundant electroactive sites in the interior tubular vessels and outer surfaces for ultrasensitive detection of NA in living cells such as PC12. The CNNB biosensor electrodes showed efficient electrocatalytic activity, enhanced kinetics for electrooxidation of NA, and fast electron-transfer between electrode–electrolyte interface surfaces, enabling synergistic enhancement in sensitivity, and selectivity at low-detectable concentration of ~ 6 nM and reproducibility of broccoli-shaped NA-electrodes. The integrated CNNB biosensor electrodes showed evidence of monitoring and screening of NA released from PC12 cells under K⁺ ion-extracellular stimulation process. The unique features of CNNB in terms of NA-selectivity among multi-competitive components, long-term stability during the detection of NA may open their practical, in-vitro application for extracellular monoamine neurotransmitters detection in living cells.

Keywords: Noradrenaline; Biosensors; Broccoli-shaped hierarchy; Electrochemical screening; living cells.

1. Introduction

Electron-transfer processes in molecular assemblies at the nanoscale are of prime importance for fundamental biological processes, as shown by insightful studies from bioinorganic chemists (Dempsey et al. 2010). They are also key processes for applications in nanotechnology, such as in the construction of functional devices on surfaces (Love et al. 2005), in engineering supramolecular redox sensors (Fujimoto et al. 2004), and modifying surfaces, for example in the fabrication of modified electrodes. Finally, the inner-sphere components in electron-transfer processes can operate biomimetic catalytic steps involved in numerous oxidation reactions.

Adrenaline (A), noradrenaline (NA), and dopamine (DA) are biogenic amines possessing a catechol ring, with the name catecholamine (CA) given to these substances. CAs play an important role in neurotransmission and other physiological processes (Bergquist and Silberring 1998; Braestrup et al. 1974; Knigge et al. 1999). Higher-than-standard levels of CA will affect the cardiovascular system, leading to high blood pressure and myocardial infarction, and lower levels of CA causing low blood pressure. Noradrenaline is a hormone secreted mainly from the adrenal medulla, and is regarded as a metabotropic neurotransmitter in the sympathetic nervous system from nerve endings and some areas of the cerebral cortex. Furthermore, NA is a significant transmitter in many parts of the central nervous system, where it is engrossed in emotional arousal, blood pressure regulation, and mood disorders. Actually, low levels of NA are associated with depression (Barrick et al. 1997).

CAs, especially noradrenaline, determination from dopaminergic cell populations as well as from striatal brain slices was performed by some variable analytical techniques including fluorescence microscopy (Wachman et al. 2004), high-performance liquid chromatography (Zhang et al. 2003), capillary electrophoresis (Lapainis et al. 2007), and spectrophotometry (Nasirizadeh and Zare 2009). However, most of these techniques are expensive; they also require sophisticated instruments to maintain and run, and the procedures for preparation of biosensors are rather time consuming. The PC12 cell line was used for neurotransmitters release because they possess similar characteristics to that of mature sympathetic neurons (Lapainis et al. 2007). Electrochemical methods have appeared to be suitable and more often employed in clinical analysis to determine the concentration of a CA or all of them owing to easy operation, cost effectiveness, and sensitivity to real-time monitoring of the targets in nano-molar concentrations. Haematoxylin electrodeposited on a glassy carbon electrode and molybdenum(IV) carbon nanotube complex-modified CPE were used as selective NA in the presence of acetaminophen and folic acid (Akhgar et al. 2012; Amiri-Aref et al. 2014; Beitollahi

and Sheikhshoae 2011). Simultaneous determination of noradrenaline with other coexisting molecules like ascorbic acid, acetaminophen, tryptophan, xanthine, and caffeine on modified glassy carbon electrode or modified carbon paste electrode was established (Beitollahi and Mohammadi 2013; Chandra et al. 2013; Knez et al. 2006; Taei and Jamshidi 2017).

Metal-oxide semiconductor nanomaterials are promising functional materials in the biosensing field because of their good biological compatibility, large surface area, special physical and chemical properties (Cherevko and Chung 2010; Irwin et al. 2008; Li et al. 2008). Semiconductor metal oxides have changing valence states, such as CuO, NiO, Co₃O₄, etc., which can be explored to construct effective sensors (Dong, 2012; Kim, 2004; Xiang, 2002). Among these materials, NiO, a p-type semiconductor with a high isoelectric point of approximately 10.7 was studied intensely because of its high chemical stability, electrocatalysis, electron transfer capability, and good biological compatibility (Dong et al. 2011; Liu et al. 2013; Salimi et al. 2007; Xiang et al. 2002; Yang et al. 2011). However, most of these electrodes have drawbacks of low sensitivity and poor selectivity caused by surface poisoning. To overcome these problems, carbon nanomaterials such as graphene (Fu et al. 2015; Ju et al. 2012), carbon nanotubes, (Ghosh Chaudhuri and Paria 2011) and ordered mesoporous carbon were combined with metal oxides, and the resulting composites were used to fabricate biosensors with improved sensing performance because these carbon nanomaterials exhibit large specific surface areas and good electrical conductivity (Wang and Hu 2014).

Carbon based materials like carbon dots, carbon nanospheres expose the electrode surface a greater fraction sites that are catalytically active to enhance the kinetics of ions and electron transport at the electrode–electrolyte interface (Ma et al. 2014). As example of metal or metal oxides carbon materials as biosensing materials, NiO@carbon–nitrogen dot electrodes was prepared and used as glucose sensors (Zhang et al. 2015), NiAl-LDH carbon dots as acetylcholine sensing (Sun et al. 2011), NiCo N-doped carbon nanoplates for simultaneous AA, UA, and DA (Zhang et al. 2015), CuO@3D graphene foams for ultrasensitive ascorbic acid detection (Ma et al. 2014), Au@carbon dots chitosan composite film for dopamine (Huang et al. 2014), and size-selected Pt@graphene/nanocomposites for simultaneous detection of ascorbic acid, dopamine, and uric acid (Sun et al. 2011).

In this paper, designing of modified electrode with high electrocatalytic activity and extensively NA monitoring secreted of from living cells was developed based on

C-, N-doped NiO broccoli-like hierarchy (CNNB). The unique geometrical and morphological structure which clearly exhibited electrocatalytic performance because of a broccoli-like hierarchy with single-head (NB-1) structure, and two asymmetric heads spread out in the opposite direction and connected with trunk (NB-2). The vertical alignment of the tubular pips throughout the entire broccoli head structure is the key role for the fast electron transfer, diffusion and electrocatalytic activity of NB modified electrodes, where the head surface is like a sea urchin surface and consists of a thick nanotube at its ends. The CN nanospheres doped NB with homogeneity at outer and entire head nanotubes, leads to facilitate the interaction between the biomolecules and the active catalytic surface sites. The CNNB shows analytical integration process for detection of mono-biomolecules such as AA, DA, A, UA and NA with highly impact on monitoring of NA. The integrated CNNB biosensor electrodes showed monitoring and screening of NA released from PC12 cells under K^+ ion-extracellular stimulation process. The CNNB can be employed for the application of in vitro detection of NA released from living cells and matched with 4',6-diamidino-2-phenylindole (DAPI).

Scheme 1

Experimental

2.1 Synthesis of CNNB-1 and CNNB-2

Nickel oxide broccoli like with single head (NB-1) and with asymmetric double head (NB-2) were fabricated via one-pot hydrothermal synthetic approach. The synthesized NB were prepared according to the following procedure: 1 mM of $Ni(NO_3)_2 \cdot 6H_2O$ was dissolved in a 100-mL volumetric flask containing 15 mL deionized water and stirred until dissolved at room temperature. Then, 15 mL of 1 mM solution of $(NH_4)_2HPO_4$ in deionized water was added to the stirred solution of $Ni(NO_3)_2 \cdot 6H_2O$ with a definite flow rate to control the shape (see supporting information, Scheme S1). The prepared solution was transferred into a 100-mL Teflon-lined stainless-steel autoclave, sealed and maintained at 160 °C for 8 h. After the required time, green precipitate appeared because of NiO formation. The precipitate was then rinsed with ultrapure water/absolute ethanol to remove the soluble impurities. The as-made NiOOH samples with different hierarchal structures were dried in an

oven at 80 °C and annealed at 400 °C for 4 h to obtain NiO broccoli like structures with single head (NB-1) and asymmetric double heads (NB-2).

Carbon-nitrogen nanospheres doped NB-1 and NB-2 were constructed as follows: 60 mg of prepared NB was dispersed in 100 mL of tris-buffer solution (pH 8.5) with ultrasonication for 2h followed by the addition of purified aniline (20 mM). Next, 20 mM of ammonium peroxydisulfate solution dissolved in 0.1 M HCl was added dropwise to the stirred solution to perform the polymerization reaction at 0 °C. The composite materials were stored for 12 h at room temperature, and the obtained aniline-polymerized NB samples were washed several times with deionized water. Following the same procedure, the polymerization was repeated three times. Finally, the polyaniline-coated NB was calcined at 500 °C for 4 h in an argon atmosphere to obtain C-N nanospheres doped NB.

2.2 Cell culture

PC12 cell line was obtained from PC12 (ATCC® CRL1721™) and was cultured by incubation under 5% CO₂ at 37 °C in Dulbecco's Modified Eagle's Medium containing 5% fetal bovine serum, 10% heat-inactivated horse serum. The culture medium was replaced every 3 to 4 days.

3. Result and discussion

The controlled synthesis of morphological growth of microstructure NB is combined with building nanostructures by using structure-directing agent templates (ammonium hydrogen phosphate) under hydrothermal treatment (HT) conditions (see scheme S1). Generally, the initial precursor (Ni(NO₃)₂·6H₂O, (NH₄)₂HPO₄) and the as-obtained broccoli-like construction NB with single (1) or asymmetric double head (2), can be produced from successive reactions. Briefly, the (NH₄)₂HPO₄ hydrolysis generates active OH⁻ and PO₄³⁻ anions during HT process. These anions subsequently reacted with Ni²⁺ ions to form (i) NiOOH frameworks, (ii) broccoli-shaped hierarchy, and (iii) formation of tubular-like needles-decorated the broccoli structures. The time-dependent, dropwise addition of PO₄³⁻ anions with a definite rate flow not only controlled formation of hierarchical NiO broccoli structures, but also the morphological shapes of the broccoli heads, as shown in scheme S1. The PO₄³⁻ anions possess massive negative charges which may act as a mediator for creation of tubular branches that spread out along the broccoli head formation. The electrostatic binding between positive-charged Ni²⁺ ions and negative-charged PO₄³⁻ ions was a driven force to create broccoli-shaped structures with head

and trunk (see Figure 1 & Scheme S1). As a result, the time-dependent addition of PO_4^{3-} anions play key roles in the formation of broccoli-shaped NiO architecture with a single or an asymmetric double head that connected by a trunk or a dipole rod. Head construction may also be attributed to the stereo PO_4^{3-} shape in its solution, which directly simulates the binding with Ni^{2+} and then the crystal growth depth along the entire structures. Carbon-nitrogen nanospheres were doped along the hierarchical NiO structures without distortion. During the doping process, a thin film of polyaniline was polymerized at 0 °C after dropwise addition of potassium persulfate with continuous stirring. Potassium persulfate generates the free radical monomer, forming a homogenous black precipitate at NB surface. Carbonization of polyaniline which acts as the nitrogen and carbon source at 500 °C in Ar gas flow lead to homogenous C-N nanospheres doped NiO.

3.1 Featured of CNNB-1 and CNNB-2

Well-controlled morphology and high stable construction with high crystalline order of NB formation was provided using field-emission scanning electron microscopy (FE-SEM) and transmission electron microscopy (TEM) images. Fig. 1 shows the FE-SEM and scanning transmission electron microscopy (STEM) of the prepared materials at different flow rates as in scheme S1, and the formation of CN-nanospheres at its surface lead to the formation of NB with asymmetric double heads (NB-2) and symmetric head (NB-1) broccoli like morphology. Fig. 1A illustrates the FE-SEM of each unit of NB-1 is like broccoli with a head and a trunk. Focusing on varied points of view demonstrate the homogeneity and unity of the new structure of NB with a stable formation, as in the vertical back of view for NB-1 (B) and CNNB-1(C). High-magnification FE-SEM images (B) represent the following dimensions of the NB-1; average head diameters ranging from 3 μm to 4 μm and trunk diameter 1 μm to 1.5 μm . Fig. 1C shows the homogeneity of carbon-nitrogen nanospheres at the NB-1. The head construction shows an exceptional construction obtained from TEM in Fig. 1D, where the end surface is like a hedgehog's skin, consisting of thick nanoneedles spread from the inner trunk to the outer surface with formation of tunable vessels. The formation of NB with two heads spread out in opposite sides and connected by a trunk in between is shown in scheme S1 (Figs. 1E–1G). Figs. 1E and 1F show the FE-SEM of another construction of NB which is broccoli shaped with two heads and one trunk. Vertical capturing alignment for one unit of NB-2 showed the structure stability and head morphology.

Further confirmation of a stable NB-2-unit construction is shown in Fig. 1F, showing two heads and a trunk; the bigger head size was approximately 5 μm to 6 μm , while the smaller

one was in the range of 2 μm to 2.5 μm and the trunk size was in the range of 1 μm to 1.5 μm . The FE-SEM image of CNNB broccoli-like hierarchy shows evidence of the formation of a unique morphology. The microscopic images show the formation of well-aligned nanotubes at the surface ends of the whole head that were like a jagged surface. High magnification using high-angle annular dark-field (HAADF)-STEM focusing on the tubes at the head surface ends shows the complete morphological constructions (Figs. 1H and 1I). The head nanotube shape is confirmed by HAADF-STEM and the tube size is approximately 20 nm, with CN homogenous covering the surface of NB. Electron diffraction (ED) focusing on nanotube surfaces reflects the degree of the crystalline structure of NB, as shown in Figs. 1J and its inset, 1K, and 1L. The nanotubes surface is a highly crystalline surface as shown in Figs. 1J–1L, focusing on the middle of the tube surface (K), deep inside, and at the edges around the (110) crystal plane. Confirmation from ED resolution of low- and high-index lattice planes of $(-1-11)$, (002) , $(1-11)$, (-220) , $(-11-1)$, $(00-2)$, $(1-1-1)$, and $(2-20)$ fringes around the bottom $\{110\}$ -principle zone-dominant plane was shown in the inset of Fig. 1H. Thus, the designed materials possess i) a smooth surface, which has a significant effect on the contact surface between the electrolyte and the designed electrode surface with enhancing the fast response of targets, ii) numerous number of active sites with exposure of a whole NB unit for the opposite electrolyte, because of the unique morphology (head with a trunk or two heads with a trunk). The intrinsic catalytic activity was increased, related to the unique construction of each unit of NB which was directly decoded as active sites.

Figure 1

Sharp and well-resolved diffraction peaks for the NB is found in the wide-angle X-ray diffraction (WA-XRD) patterns as shown in Fig. 1N which was consistent with JCPDS no. 01-089-5881 (i.e., a face-centred cubic $Fm\bar{3}m$ symmetry with the lattice constant $a = 8.35 \text{ \AA}$) (Akhtar et al. 2016; Khairy et al. 2012). However, WA-XRD profile of CN-nanospheres doped NB-1 and NB-2 (Fig 3B) were found to keep the characteristic diffraction peaks of face-centered cubic NiO (JCPDS no. 01-089-5881), along with a broad peak at $2\theta = 24.61$, indicating the existence of carbon (Dong et al. 2011).

To confirm the existence of carbon, material structure, and sample functional group, Raman shift spectrum was used at the excitation wavelength of 532 nm (Fig. S1A). The peaks at 532 cm^{-1} , 760 cm^{-1} , and 1085 cm^{-1} were attributed to one phonon (1P)(TO), (2P) 2TO and (2P) 2TO modes and 2LO (longitudinal optical) modes,

respectively, indicating the presence of pristine NiO for NB samples. The CNNB provides two distinct peaks in CNNB-1 and CNNB-2 corresponds to D ($\sim 1366\text{ cm}^{-1}$) and G ($\sim 1500\text{ cm}^{-1}$) bands originating from the disordered carbon and sp^2 cluster, respectively (Kavitha and Yuvaraj 2011) (for more details see supporting information). The N_2 adsorption–desorption isotherm of NB samples featured type IV with H2-type hysteresis loop, NLDF model as in Fig. 1M. These data confirmed that NB-2, NB-1, and CNNB-2 has two types of pores (meso- and macropore) and provides the hierarchical structure of the prepared samples while mesoporous structure is dominant for CNNB-1 with high surface area (for more details see supporting informations). Elucidations of surface components of CNNB as well as NB were performed by XPS measurements, where high-resolution XPS spectra of the Ni 2p, O 1s, C 1s, and N 1s peaks were performed for complete construction formations (for more details see supporting informations).

3.2 Surface configuration of microscopic CNNB-1 and CNNB-2

The $\{110\}$ and $\{101\}$ close-packed plane and its surface atomic configurations, electron density difference maps, and pulse surface electrons in continuous generation modes around the NB-1 and NB-2 active sites are illustrated in Fig. 2A. The surface structure has a mesoporous framework around $\{110\}$ planes, which increases the actively energetic surface coverage for easy diffusion which leads to high electron transport shown in the electrolyte surface interfaces. Fig. 2B illustrates the continuous electron streams on the top-level of $\{110\}$ orientation distributed closely to a central and focal point surface around the Ni^{2+} and O^{2-} vacancy sites of NB-1, and surface-representing localized network of the confinement electrostatic potential elevated to antedate the surface charge density around O and Ni atoms and effective potential molecules to Ni^{2+} site binding. In addition, Figs. 4(C and D) reveal that the $\{110\}$ -surface energy, the atomic O and Ni density, CN surface concentration, and the $\{110\}$ -surface activation energy of CNNB-1 are the key elements that affect the highest sensitivity of noradrenaline. The CNNB-1 geometric molecule-to-surface orientation generated numerous accessible surface sites and flexible interactions and thermodynamically stable bindings. Figs. 2E and 2F show that the $\{110\}$ and $\{101\}$ -top-surface around double-layer surfaces provide high energy electron surfaces formed along the entire NB crystal structure directed along $\{110\}$ and $\{101\}$ surface exposure, particularly at the 4- Ni^{2+} -top surfaces (E) which enhances the electrocatalytic activity of Ni^{2+} with the target molecules. The surface configurations of CNNB-1 hierarchy oriented with exposed high-index facets along $\{110\}$ domains can feasibly create dense Ni^{2+} atoms and

more electron-rich O^{2-} vacancy sites, producing more efficient electron transport and biomolecules-to-surface binding along the {110} exposed plane.

Figure 2

3.2 Electrocatalytic activity of the CNNB biosensor electrodes

We initially investigated the electrochemical behavior of the CNNB-2 and CNNB-1 fabricated at ITO electrode. Cyclic voltammetry (CV) technique was performed in 0.1 M PBS (pH 7.0) containing 1 mM $[Fe(CN)_6]^{3-}$ within the potential range of 0.0 V to 0.6 V (vs. Ag/AgCl) and at a scan rate of 100 mV/s (Fig. S3A). $[Fe(CN)_6]^{3-}$ were used as a redox probe to investigate various factors including electronic properties, surface structure, and surface chemistry that affect the charge kinetics of the selected electrodes (Kavitha and Yuvaraj 2011). Fig. S3A shows that the redox peak separation (ΔE_p) values of the CNNB-1 (69 mV) was lower than that of the CNNB-2 (80 mV) electrodes, which can be attributed to the enhanced ion transmission performance at the electrode–electrolyte interface, thereby engaging greater fractions of catalytic active sites on the surface of the electrode for the Faradaic redox reaction.

The electron transfer and electron diffusion properties of CNNB-1 and CNNB-2 were investigated using impedance spectroscopy measurements (EIS) (Fig. S3B). In an EIS measurement, the semicircle diameter reflects the electron transfer resistance (R_{et}) of the electrode and the line reflects the diffusion of the electroactive species. In general, a large semicircle means a high charge transfer resistance of the electrode, implying a low electron transfer rate (higher resistivity) (Chen et al. 2014). Typical Nyquist impedance plots of CNNB-2 and CNNB-1 biosensor electrodes in 0.1 M PBS (pH 7.0) are shown in Fig. S3B. The semicircle of the CNNB-1 electrode shows further decrease than CNNB-2 biosensor electrode with extremely low R_{et} value and high conductivity. CNNB-1 has high catalytic activity and low resistance with high ion diffusion than CNNB-2, which may be related to high surface area, dominant mesoporous structure, highly dense electronic charge with dominant {110} plane and low surface tension along with longitudinal axial orientation of contact Ni^{2+} atoms with NC surface clouds coverage.

3.3 Electrochemical behaviour of CNNB-2 and CNNB-1 for mono-biomolecules

The electrochemical behaviours of mono-biomolecules such as NA, AA, A, DA, and UA on the CNNB-2 and CNNB-1 were measured using differential pulse voltammetry (DPV) in 0.1 M PBS solution pH 7 at pulse height of 60 mV and pulse width 25 ms. Fig. 3A shows the catalytic oxidation of 5 μ M NA on CNNB-2 and N- CNNB-1. A significant DPV peak observed at applied potential 0.17 V for CNNB-2 and CNNB-1, which correspond to the oxidation of NA to o-quinone forms and provides that CNNB-1 has more sensitivity than CNNB-2. The same behaviour is observed for 0.5 mM AA, 10 μ M DA, 10 μ M A, and 0.2 mM UA. The catalytic oxidation current of CNNB-1 is higher than that of CNNB-2 at onset potentials 0.05, 0.31, 0.12 and 0.47 in PBS pH 7 for AA, DA, A, and UA, respectively as shown in Figs. 3(B–5D). The modified electrode showing high selectivity along with visualizing the peak separation (ΔE) between the coexisting molecules compared with NA were $\Delta E_{AA-NA} = 120$ mV, $\Delta E_{A-NA} = 50$ mV, $\Delta E_{DA-NA} = 140$ mV, and $\Delta E_{AA-NA} = 300$ mV. These findings show that the CNNB-1 biosensor electrode is sensitive for AA, A, DA, UA, and NA caused by the enhanced electrocatalytic properties and the deep diffusion of molecules show its pores, with axial contact along with {110} plane with surface coverage charge clouds on the surface.

3.4 Electrochemical detection of mono-biomolecules on CNNB-1 biosensor

The individual detection of mono-biomolecules such as NA, AA, A, DA, and UA on CNNB-1 biosensor electrode was examined by DPV in PBS pH 7 at a pulse height of 60 mV and a pulse width of 25 ms. As shown in Fig. S4A, the current response of UA increases with increasing UA concentrations from 25 μ M to 600 μ M; the linear regression equation was $\{I (\mu A) = 0.73 [UA] (\mu M) + 26.62; R^2=0.99\}$; therefore, the detection limit was 15 μ M based on regression equation ($S/N = 3$). For AA, the current response increased with increasing the AA concentrations from 50 μ M to 2 mM; the linear regression equation was $\{I (\mu A) = 0.021 [AA] (\mu M) + 19.7; R^2=0.99\}$ and the detection limit was calculated to be 36 μ M as shown in Fig. S4B and its inset. DPV of DA, A, and NA on CNNB-1 biosensor electrode in 0.1 M PBS (pH 7.0) shown in Figs. S4(C–E). The oxidation peak currents for DA, A, and NA increased proportionally with increasing concentration in a range from 0.1 μ M to 32 μ M, indicating that the CNNB-1 biosensor electrode can be used for the determination of dopamine,

adrenaline, and noradrenaline. By plotting the concentration versus the current for DA, A, and NA, the linear regression equations are $I(\mu\text{A})= 0.64+2.05 [\text{DA}] (\mu\text{M})$ ($R^2=0.988$), $I(\mu\text{A})= 22.31+1.46 [\text{A}] (\mu\text{M})$ ($R^2=0.979$) and $I(\mu\text{A})=44.79 + 29.2 [\text{NA}] (\mu\text{M})$ ($R^2= 0.977$). The detection limit was calculated to be 2.6, 2.86, and 0.35 μM for DA, A, and NA, respectively. Selectivity of CNNB-1 biosensor electrode for NA was clearly obtained from the detection limit of each of the analytes and illustrated in Fig. S4G, where the peak current response was high for NA compared with the other analytes at the same concentration. Furthermore, no current response was found for AA and UA at the obvious concentrations of NA. These data illustrated the selectivity of CNNB-1 for biosensing of NA molecule.

Figure 3

3.5. Wide-range sensitivity and long-term stability of CNNB-1 biosensor electrodes

Studying of the NA-sensitivity on CNNB-1 at low concentrations; chronoamperometric studies were performed at applied potential 0.17 V in PBS (pH 7). Fig. 4A shows the amperometric response of NA as step addition of 0.5 μM . With the spiking of NA concentrations, the amperometric current response was increased with fast response time within 10 s which release the superior sensitivity of CNNB-1 biosensor electrode for monitoring of NA. The linear regression equation was expressed as: $I (\mu\text{A}) = 4.32+22.67 [\text{NA}] (\mu\text{M})$, with correlation coefficient of 0.999 (Fig. 4B). The relative standard deviation (RSD) was estimated to be 2.5% with low detection limit = 6 nM. CNNB-1 biosensor electrode exhibits superior sensitivity for NA when compared with other electrodes as shown in Table S1, where CNNB-1 provides highest sensitivity compared to the other modified electrodes. Thus, CNNB-1 biosensor electrode represents NA biosensor with high sensitivity and selectivity.

The reproducibility of the CNNB-1 biosensor electrode was evaluated. In such experimental protocols, the current responses are examined for multiple (≥ 5) CNNB-1 biosensor electrode in 10 μM NA concentration at the optimum sensing conditions of 0.1 M PBS (pH 7) and applied potential of 0.17 V (vs. Ag/AgCl) at 20 °C. The RSD of the five amperometric response assays ranged within 1.7% to 2.25%, as evidenced by the fitting plot of the response current graphs (Fig. S5). To confirm the reusability of CNNB-1 biosensor electrode, current responses as a function of five different samples

with constant concentration of NA (10 μM) were measured repeatedly after every washing of CNNB-1 biosensor electrode with distilled H_2O for three times at the optimum sensing conditions (Fig. S5). Thus, the reused CNNB-1 biosensor electrode showed high sensing response efficiency (i.e., 98%) despite five reuses/cycles.

Figure 4

3.6 Monitoring of NA released from living cells (PC12) at CNNB-1 biosensor electrode

For the evaluation of neurological disorder (i.e., schizophrenia) on the basis of disruption level of neurotransmitter, we selected healthy (PC12) cells, which is similar to human neuronal cells. We assessed the suitability of the designed CNNB-1 biosensor electrode for control monitoring of an in vitro NA released from PC12 cells (cells with extracellular dopamine). Many time-dependent methods using sophisticated techniques that do not have real-time responses have been used to monitor the NA release from cells, which usually require hours of work for sample collection and NA recognition using HPLC purification and mass identification (Lapainis et al. 2007; Nasirizadeh and Zare 2009; Wachman et al. 2004; Zhang et al. 2003). In comparison, Fig. 4(B-E) depicts the real-time recording using CNNB-1 biosensor electrode, where NA released from PC12 was monitored with a current change within few seconds by using amperometric measurements.

K^+ induced noradrenaline released from PC12 cells was monitored through amperometric response under an applied potential of 0.17 V in 0.1 M PBS pH 7 (Figs. 4A and 4B). First, we directly investigate the various concentrations of noradrenaline in 0.1 M PBS solution (pH 7.0) as shown in Fig. 4C, where the amperometric response increased with step adding 1 μM NA noradrenaline. Similarly, we observe an amperometric response for NA released from PC12 as a constant addition of spiked 1 μM of NA with a supernatant of PC12 incubated with 30 mM KCl for various times (2, 5, 10, 20, and 30 min) (Fig. 4DB). Fig. 4E shows the column plot of concentration of NA versus the current for CNNB-1 biosensor electrode in PBS (pH 7) for spiking NA only and NA with induced NA from PC12. Fig. 4E shows that the current response of NA with induced NA from PC12 was higher than that of spiked NA only. Cell membrane depolarization was reported by K^+ extracellular simulation in which the cell membrane depolarized and induced an influx of Ca^{2+} and Na^+ through the opening of voltage-sensitive Na^+ and Ca^{2+} channels (Shinohara et al. 2013). Increasing the level of intracellular Ca^{2+} enhances the release of NA from large dense core vesicles of the cells. The

cells were simulated by K^+ to depolarize the cells as recorded from Fig. 4D and represented in column 4E (blue line). The released NA from PC12 increased as the incubation time was increased with 30 mM K^+ .

For further confirmation, PC12 cells were visualized using laser scanning confocal microscopy measurements after confirming the active wavelength region (Fig. 5). An in vitro model was adapted to study the interaction of CNNB-1 (20 $\mu\text{g}/\text{mL}$) and PC12 cells (5×10^5 cells/mL). Results indicate the positive detection of the released extracellular NA due to signal enhancement after incubation with CNNB-1 (Fig. 5D). DAPI (0.1 $\mu\text{g}/\text{mL}$) were used for PC12 cells nuclear counterstaining which indicates the localization within the cell and incubated cells with 30 mM K^+ (Fig. 5A&C). Fig. 5(B&D) shows the co-localization and matching between CNNB-1 and DAPI counter stain which reflects a high degree of matching positivity and after incubation for 30 min with 30 mM K^+ . In addition, the low toxicity observed by confocal microscope visualization of the cells incubated with CNNB-1 (20 $\mu\text{g}/\text{mL}$) and control, where no damage or shrinkage on the cells membrane and the micro unit of CNNB-1 was clearly obtained with cells imaging. These results confirmed that CNNB-1 can be used as a real in-vitro model for extracellular noradrenaline detection.

Figure 5

Conclusion

Simple, sensitive, and selective biosensor electrodes were successfully developed for electrochemical determination, and screening of noradrenaline in PC12 cells. Designing of NA-electrode based on C-, N doped NB broccoli-like hierarchy (CNNB) was fabricated. The fabrication of CNNB electrodes with controlled formation of single broccoli head (CNNB-1) or two asymmetric broccoli heads spread out in opposite directions that connected by trunk (CNNB-2) show the key factors in the sensitive and selective monitoring of NA. The electrode design of spherical broccoli-heads was associated with dense nanoneedles aligned vertically along the entire trunk axes connected with spherical CNNB heads. Such jagged surface of electrode with dominant meso-tunnel-like pore structure may lead to provide multi active sites, open-spaces, and easy mass transport at the electrode surface. The active doping of the NB broccoli-like hierarchy with CN nanospheres facilitate the electron transport, and create abundant active sites inset of the tubes and outer surfaces. The CNNB biosensor provides high catalytic activity associated with the shape construction with doping of C-N nanospheres. The CNNB-1 biosensor exhibits high selectivity, sensitivity, stability, and reproducibility with low

detection limit up to ~ 6 nM for monitoring of NA. Signalling and monitoring of NA released from living cells (PC12) successfully proceeds at the CNNB-1 biosensor with high sensitivity and selectivity. The unique morphology of CNNB-1 for NA-selectivity among interfering molecules, may open their practical, in-vitro application for extracellular NA detection in living cells

References

- Akhgar, M.R., Beitollahi, H., Salari, M., Karimi-Maleh, H., Zamani, H., 2012. Fabrication of a sensor for simultaneous determination of norepinephrine, acetaminophen and tryptophan using a modified carbon nanotube paste electrode. *Analytical Methods* 4(1), 259-264.
- Akhtar, N., El-Safty, S.A., Abdelsalam, M.E., Shenashen, M.A., Kowarada, H., 2016. Radially oriented nanostrand electrodes to boost glucose sensing in mammalian blood. *Biosensors and Bioelectronics* 77, 656-665.
- Amiri-Aref, M., Raouf, J.B., Ojani, R., 2014. A highly sensitive electrochemical sensor for simultaneous voltammetric determination of noradrenaline, acetaminophen, xanthine and caffeine based on a flavonoid nanostructured modified glassy carbon electrode. *Sensors and Actuators B: Chemical* 192, 634-641.
- Barrick, D., Ho, N.T., Simplaceanu, V., Dahlquist, F.W., Ho, C., 1997. A test of the role of the proximal histidines in the Perutz model for cooperativity in haemoglobin. *Nature Structural & Molecular Biology* 4(1), 78-83.
- Beitollahi, H., Mohammadi, S., 2013. Selective voltammetric determination of norepinephrine in the presence of acetaminophen and tryptophan on the surface of a modified carbon nanotube paste electrode. *Materials Science and Engineering: C* 33(6), 3214-3219.
- Beitollahi, H., Sheikhshoae, I., 2011. Selective voltammetric determination of norepinephrine in the presence of acetaminophen and folic acid at a modified carbon nanotube paste electrode. *Journal of Electroanalytical Chemistry* 661(2), 336-342.
- Bergquist, J., Silberring, J., 1998. Identification of catecholamines in the immune system by electrospray ionization mass spectrometry. *Rapid communications in mass spectrometry* 12(11), 683-688.
- Braestrup, C., Nielsen, M., Scheel-Krüger, J., 1974. Accumulation and disappearance of noradrenaline and its major metabolites synthesized from intraventricularly injected [³H] dopamine in the rat brain. *Journal of neurochemistry* 23(3), 569-578.

- Chandra, P., Son, N.X., Noh, H.-B., Goyal, R.N., Shim, Y.-B., 2013. Investigation on the downregulation of dopamine by acetaminophen administration based on their simultaneous determination in urine. *Biosensors and Bioelectronics* 39(1), 139-144.
- Chen, L., Feng, M., Zhan, H., 2014. Fundamental electrochemistry of three-dimensional graphene aerogels. *RSC Advances* 4(58), 30689-30696.
- Cherevko, S., Chung, C.-H., 2010. The porous CuO electrode fabricated by hydrogen bubble evolution and its application to highly sensitive non-enzymatic glucose detection. *Talanta* 80(3), 1371-1377.
- Dempsey, J.L., Winkler, J.R., Gray, H.B., 2010. Proton-coupled electron flow in protein redox machines. *Chemical reviews* 110(12), 7024-7039.
- Dong, S., Zhang, P., Liu, H., Li, N., Huang, T., 2011. Direct electrochemistry and electrocatalysis of hemoglobin in composite film based on ionic liquid and NiO microspheres with different morphologies. *Biosensors and Bioelectronics* 26(10), 4082-4087.
- Fu, S., Fan, G., Yang, L., Li, F., 2015. Non-enzymatic glucose sensor based on Au nanoparticles decorated ternary Ni-Al layered double hydroxide/single-walled carbon nanotubes/graphene nanocomposite. *Electrochimica acta* 152, 146-154.
- Fujimoto, S., Mizuno, R., Saito, Y., Nakamura, S., 2004. Clinical application of wave intensity for the treatment of essential hypertension. *Heart and vessels* 19(1), 19-22.
- Ghosh Chaudhuri, R., Paria, S., 2011. Core/shell nanoparticles: classes, properties, synthesis mechanisms, characterization, and applications. *Chemical reviews* 112(4), 2373-2433.
- Huang, Q., Zhang, H., Hu, S., Li, F., Weng, W., Chen, J., Wang, Q., He, Y., Zhang, W., Bao, X., 2014. A sensitive and reliable dopamine biosensor was developed based on the Au@ carbon dots–chitosan composite film. *Biosensors and Bioelectronics* 52, 277-280.
- Irwin, M.D., Buchholz, D.B., Hains, A.W., Chang, R.P., Marks, T.J., 2008. p-Type semiconducting nickel oxide as an efficiency-enhancing anode interfacial layer in polymer bulk-heterojunction solar cells. *Proceedings of the National Academy of Sciences* 105(8), 2783-2787.
- Ju, J., Bai, J., Bo, X., Guo, L., 2012. Non-enzymatic acetylcholine sensor based on Ni–Al layered double hydroxides/ordered mesoporous carbon. *Electrochimica Acta* 78, 569-575.
- Kavitha, T., Yuvaraj, H., 2011. A facile approach to the synthesis of high-quality NiO nanorods: electrochemical and antibacterial properties. *Journal of Materials Chemistry* 21(39), 15686-15691.
- Khairy, M., El-Safty, S.A., Ismael, M., Kawarada, H., 2012. Mesoporous NiO nanomagnets as catalysts and separators of chemical agents. *Applied Catalysis B: Environmental* 127, 1-10.

- Knez, M., Kadri, A., Wege, C., Gösele, U., Jeske, H., Nielsch, K., 2006. Atomic layer deposition on biological macromolecules: metal oxide coating of tobacco mosaic virus and ferritin. *Nano Letters* 6(6), 1172-1177.
- Knigge, U., Willems, E., Kjær, A., Jørgensen, H., Warberg, J., 1999. Histaminergic and Catecholaminergic Interactions in the Central Regulation of Vasopressin and Oxytocin Secretion 1. *Endocrinology* 140(8), 3713-3719.
- Lapainis, T., Scanlan, C., Rubakhin, S., Sweedler, J., 2007. A multichannel native fluorescence detection system for capillary electrophoretic analysis of neurotransmitters in single neurons. *Analytical and bioanalytical chemistry* 387(1), 97-105.
- Li, C., Liu, Y., Li, L., Du, Z., Xu, S., Zhang, M., Yin, X., Wang, T., 2008. A novel amperometric biosensor based on NiO hollow nanospheres for biosensing glucose. *Talanta* 77(1), 455-459.
- Liu, M., Liu, R., Chen, W., 2013. Graphene wrapped Cu₂O nanocubes: non-enzymatic electrochemical sensors for the detection of glucose and hydrogen peroxide with enhanced stability. *Biosensors and Bioelectronics* 45, 206-212.
- Love, J.C., Estroff, L.A., Kriebel, J.K., Nuzzo, R.G., Whitesides, G.M., 2005. Self-assembled monolayers of thiolates on metals as a form of nanotechnology. *Chemical reviews* 105(4), 1103-1170.
- Ma, Y., Zhao, M., Cai, B., Wang, W., Ye, Z., Huang, J., 2014. 3D graphene foams decorated by CuO nanoflowers for ultrasensitive ascorbic acid detection. *Biosensors and Bioelectronics* 59, 384-388.
- Nasirizadeh, N., Zare, H.R., 2009. Differential pulse voltammetric simultaneous determination of noradrenalin and acetaminophen using a hematoxylin biosensor. *Talanta* 80(2), 656-663.
- Salimi, A., Sharifi, E., Noorbakhsh, A., Soltanian, S., 2007. Immobilization of glucose oxidase on electrodeposited nickel oxide nanoparticles: direct electron transfer and electrocatalytic activity. *Biosensors and Bioelectronics* 22(12), 3146-3153.
- Shinohara, H., Sakai, Y., Mir, T.A., 2013. Real-time monitoring of intracellular signal transduction in PC12 cells by two-dimensional surface plasmon resonance imager. *Analytical biochemistry* 441(2), 185-189.
- Sun, C.-L., Lee, H.-H., Yang, J.-M., Wu, C.-C., 2011. The simultaneous electrochemical detection of ascorbic acid, dopamine, and uric acid using graphene/size-selected Pt nanocomposites. *Biosensors and Bioelectronics* 26(8), 3450-3455.

- Taei, M., Jamshidi, M.S., 2017. A voltammetric sensor for simultaneous determination of ascorbic acid, noradrenaline, acetaminophen and tryptophan. *Microchemical Journal* 130, 108-115.
- Wachman, E.S., Poage, R.E., Stiles, J.R., Farkas, D.L., Meriney, S.D., 2004. Spatial distribution of calcium entry evoked by single action potentials within the presynaptic active zone. *Journal of Neuroscience* 24(12), 2877-2885.
- Wang, Y., Hu, A., 2014. Carbon quantum dots: synthesis, properties and applications. *Journal of Materials Chemistry C* 2(34), 6921-6939.
- Xiang, L., Deng, X., Jin, Y., 2002. Experimental study on synthesis of NiO nano-particles. *Scripta Materialia* 47(4), 219-224.
- Yang, S., Feng, X., Wang, X., Müllen, K., 2011. Graphene-Based Carbon Nitride Nanosheets as Efficient Metal-Free Electrocatalysts for Oxygen Reduction Reactions. *Angewandte Chemie International Edition* 50(23), 5339-5343.
- Zhang, L., Qv, S., Wang, Z., Cheng, J., 2003. Determination of dopamine in single rat pheochromocytoma cell by capillary electrophoresis with amperometric detection. *Journal of Chromatography B* 792(2), 381-385.
- Zhang, X., Yan, W., Zhang, J., Li, Y., Tang, W., Xu, Q., 2015. NiCo-embedded in hierarchically structured N-doped carbon nanoplates for the efficient electrochemical determination of ascorbic acid, dopamine, and uric acid. *RSC Advances* 5(80), 65532-65539.

Figures and scheme captions

Scheme 1. A) Confocal microscopy of PC12 incubated with 20 mM KCl providing the section of extracellular noradrenaline. B) binding of noradrenaline at the surface of CNNB-1 with corresponding {110} crystal plane. C) The oxidized form of noradrenaline which converted to quinone form with losing of $2e^-/2H^+$.

Figure 1. (A) Low magnification of FE-SEM micrograph for CNNB-1. (B) high magnification of FE-SEM for unit construction of NB-1 form vertical back of view, which obtaining the controlled formation of NB unit with head and trunk. (C) high magnification of FE-SEM for NB-1 covered by CN-nanospheres form vertical point of view. (D) HAADF-STEM micrograph focused on the head unit for clearing the surface morphology (E) FE-SEM for NB-2, clearing the difference in head sizes for each unit and confirmed by other unit which clearly represent the size of two different heads and the trunk in-between as in (F). (G) High magnification FE-SEM on the head unit of CNNB-2. (H,I) High magnification of HAADF-STEM focusing on the tubes of the top head surface, inset high-dense ED-STEM, corresponding the atomic configuration along {110} crystal planes. (J) High magnification of HAADF-STEM focusing on the ends of tubes and reflecting the crystalline surface degree, focusing on different degree of the tube at its centre (K), denser for interior head (L) and at its top edge (inset of J).(M) NLDF pore size distribution. (N) XRD patterns of NB and CNNB. Table (inset of M) shows the pore size and S_{BET} for NB-2, NB-1, CNNB-2 and CNNB-1.

Figure 2. (A) Mesoporous {110}-NB crystal facet oriented around the mesopore frameworks. The structure was tilted with 15° . The location of the frame structure along {110} plane enabled the actively energetic surface coverage for facile diffusion and strong binding with the target molecules. (B) The atomic organization of NB-1 crystal into exposed {110} surface plane. (C, D) High energy surfaces formed along the entire crystal structure directed along {110} and {101} surface exposure and CN-nanospheres clouds over Ni and O atoms for NB-1 and NB-2, respectively. (E and F) {110} and {101}-top-surface around double-layer surfaces show high energy electron surfaces formed along the entire NB crystal structure directed along {110} and {101} surface exposure, particularly at the Ni^{2+} -top surfaces with NC clouds.

Figure 3. DPV of CNNB-2 (wine line) and CNNB-1 (red line) for 0.2 mM UA (A), 0.5 mM AA (B), 10 μ M DA (C) 10 μ M A (D) and 5 μ M NA (E) in PBS pH= 7 at scan rate = 100 mVs⁻¹, pulse Hight = 60 mV, pulse width = 25 ms.

Figure 4. (A) The amperometric response of NA with successive addition from 0.5-5 μ M on CNNB-1 nanoelectrode and (B) The linear plot of concentration (μ M) Vs the current (μ A). (C &D) The amperometric response of NA addition in PBS pH=7 without and with PC12 induced by 30 mM KCl, (E) the column plot of concentration of norarenaline with (blue column) and without (green column) PC12 (30 mM KCl) Vs the current (μ A) at applied potential 0.17 V.

Figure 5. Confocal microscope images recorded at excitation wavelength of 488 nm and emission wavelength at 620 nm of control PC12 cells (A) and incubation of PC12 with 30 mM KCl for 30 min (C), PC12 cells with 20 μ g/ml CNNB-1 for 30 min (B) and incubated PC12 +20 μ g/ml CNNB-1 with 30 mM KCl for 30 min (D).

Scheme 1

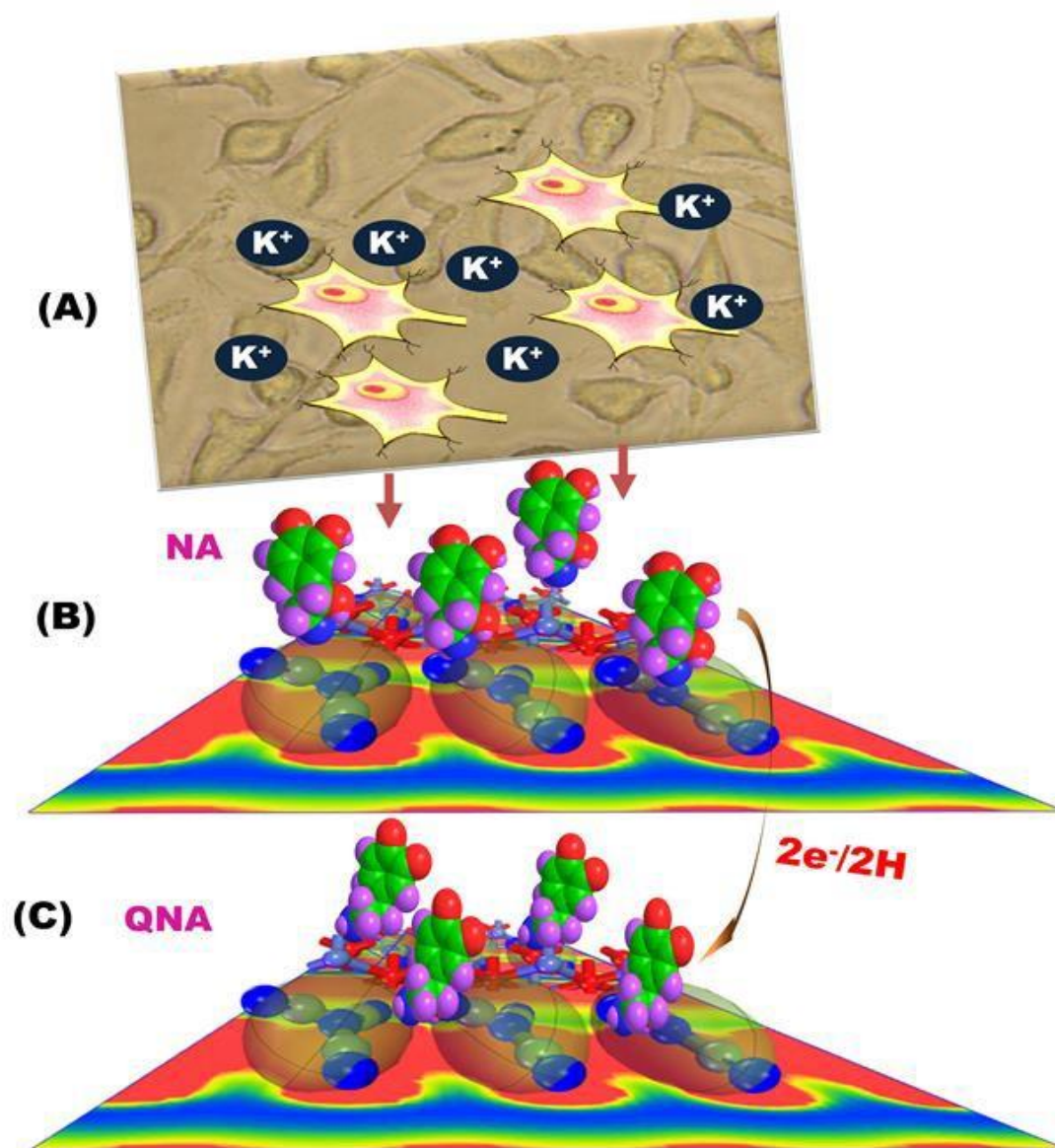


Figure 1

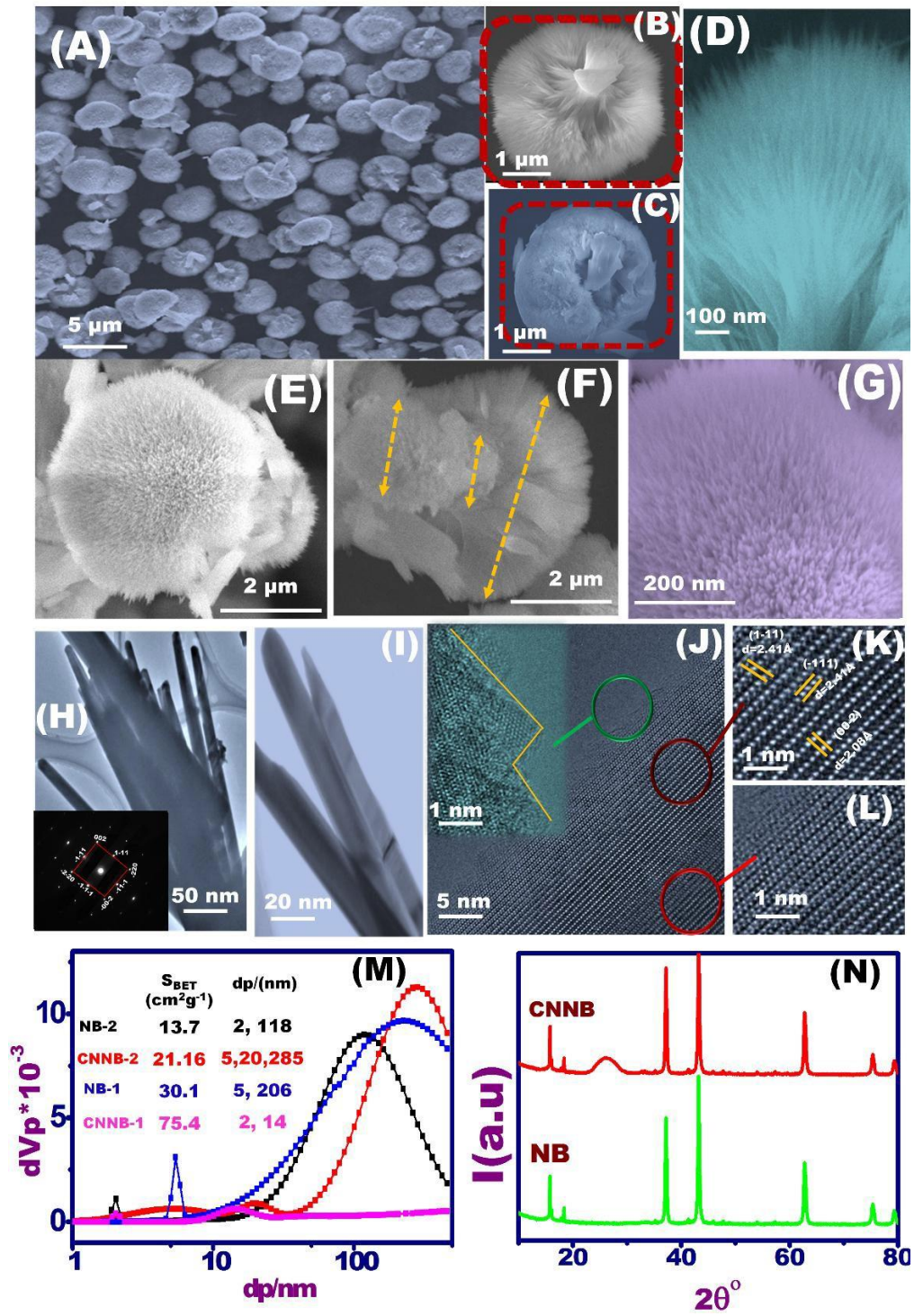


Figure 2

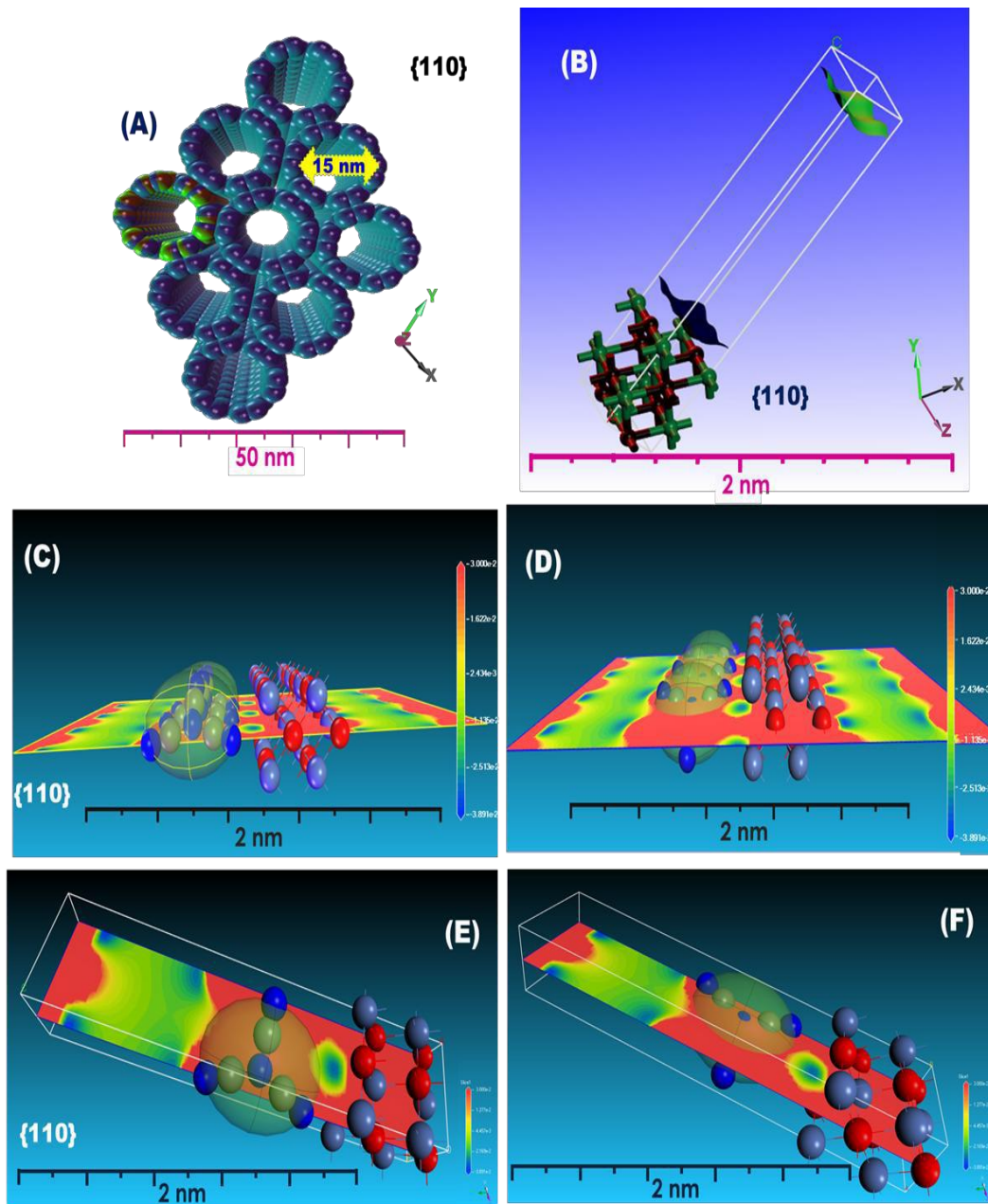


Figure 3

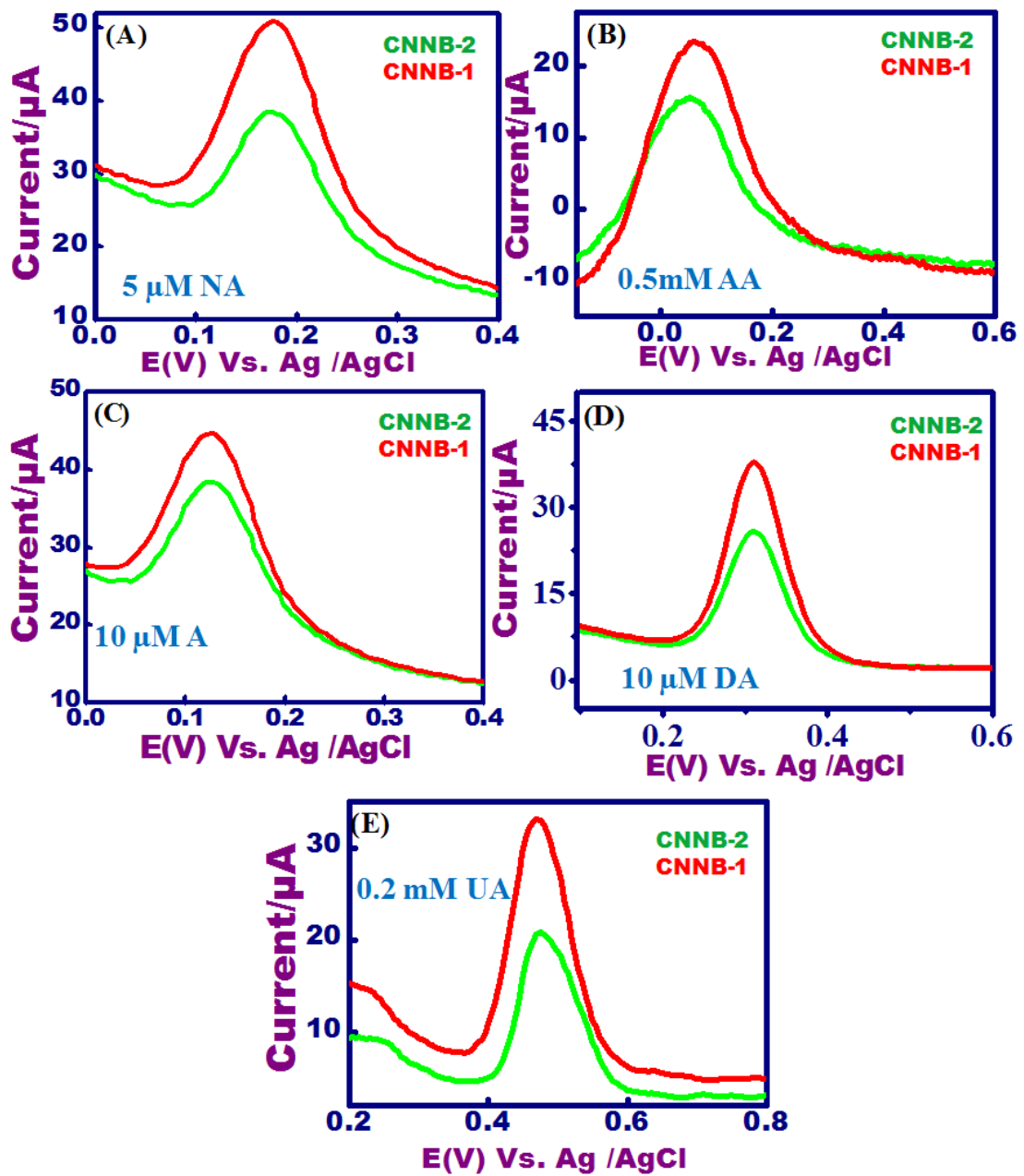


Figure 4

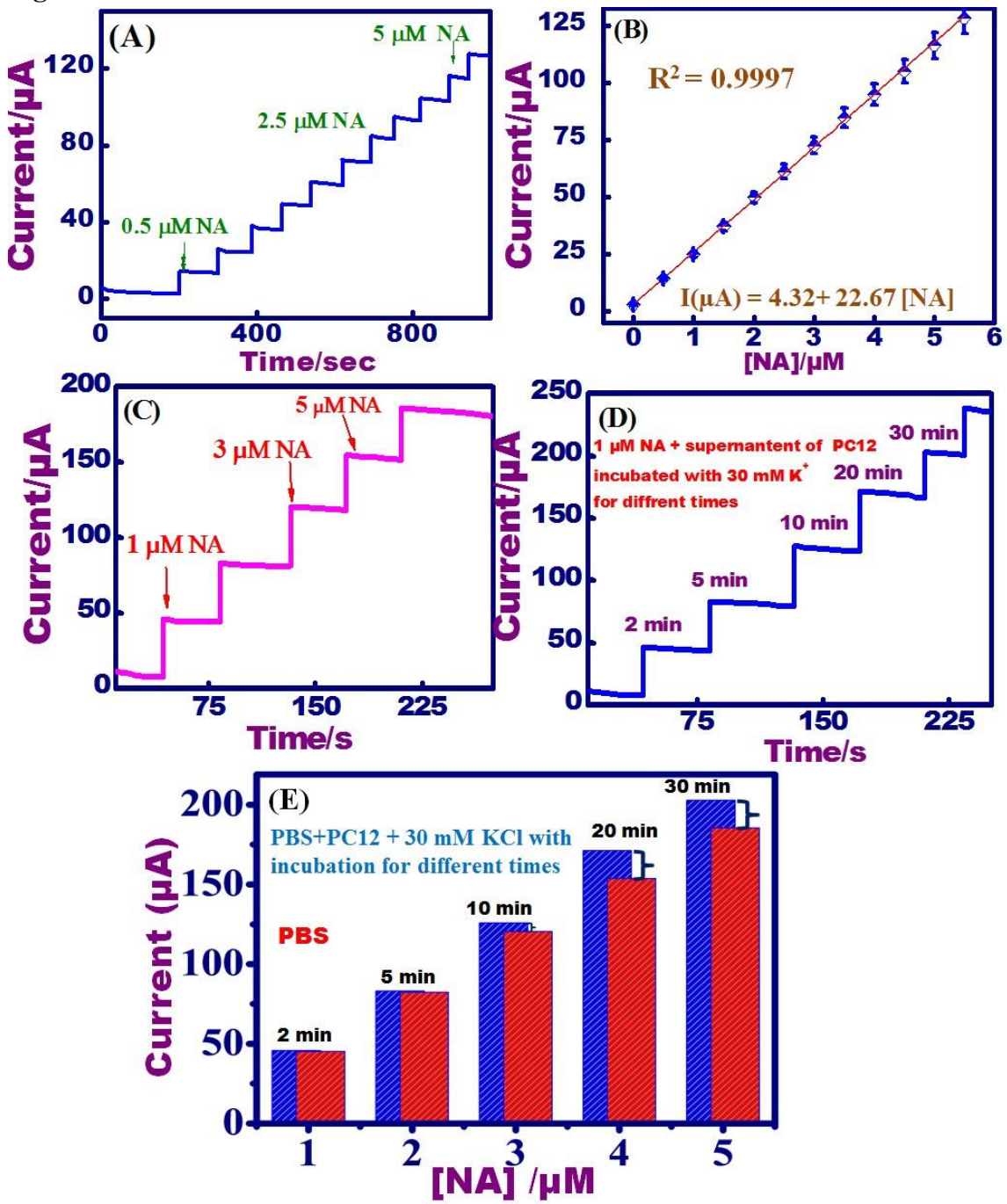
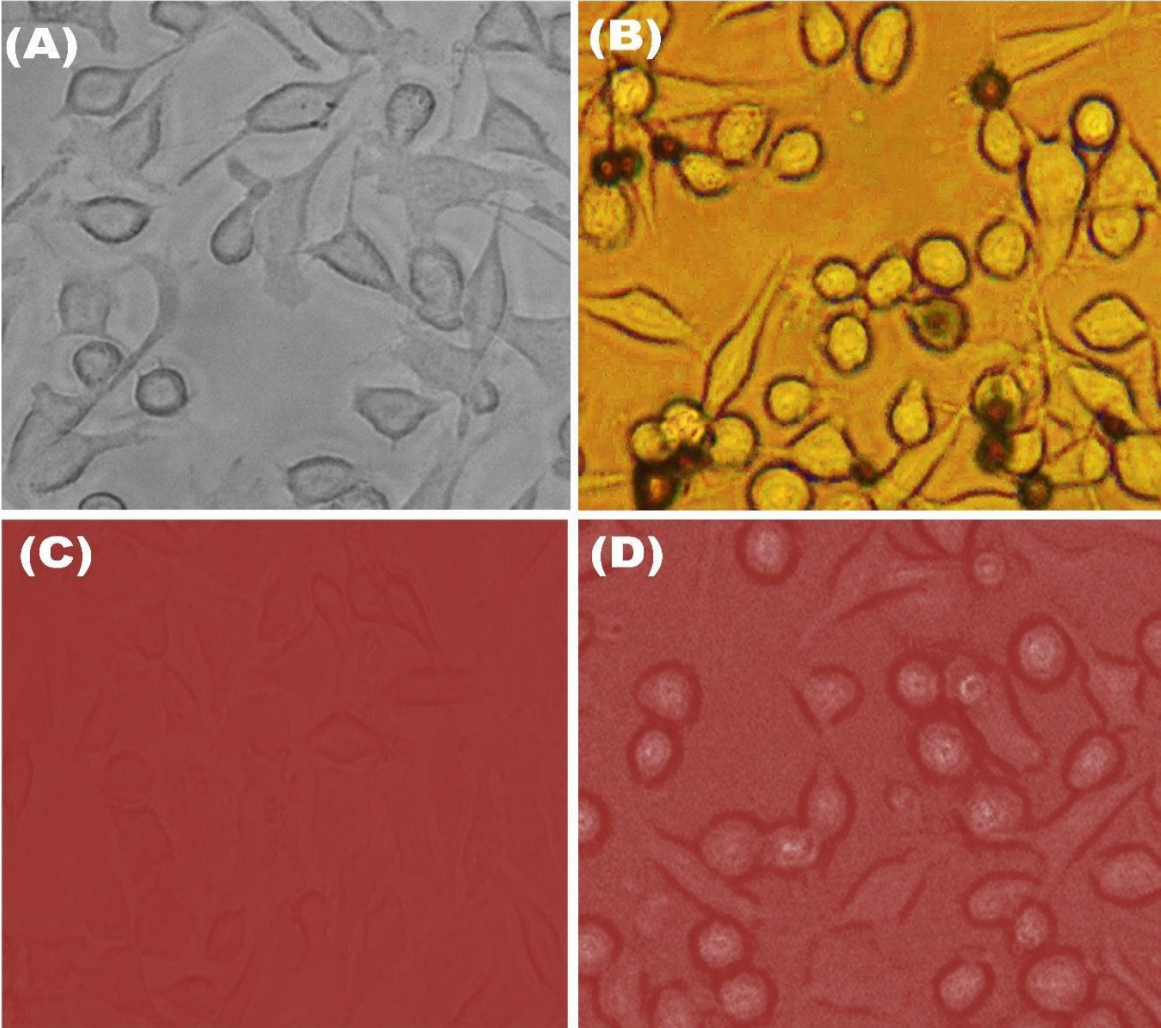
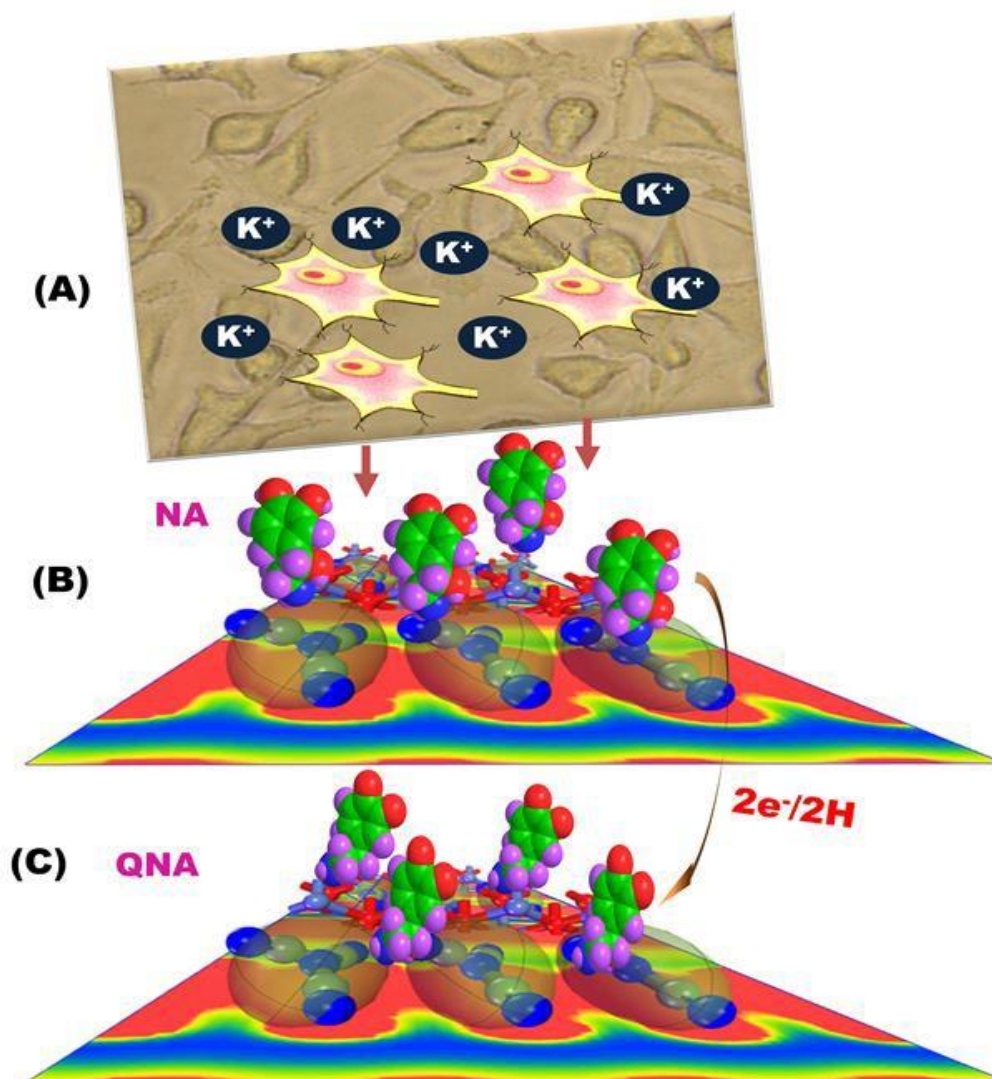


Figure 5





Scheme 1. A) Confocal microscopy of PC12 incubated with 20 mM KCl providing the section of extracellular noradrenaline. B) binding of noradrenaline at the surface of CNNB-1 with corresponding {110} crystal plane. C) The oxidized form of noradrenaline which converted to quinone form with losing of $2e^-/2H^+$.

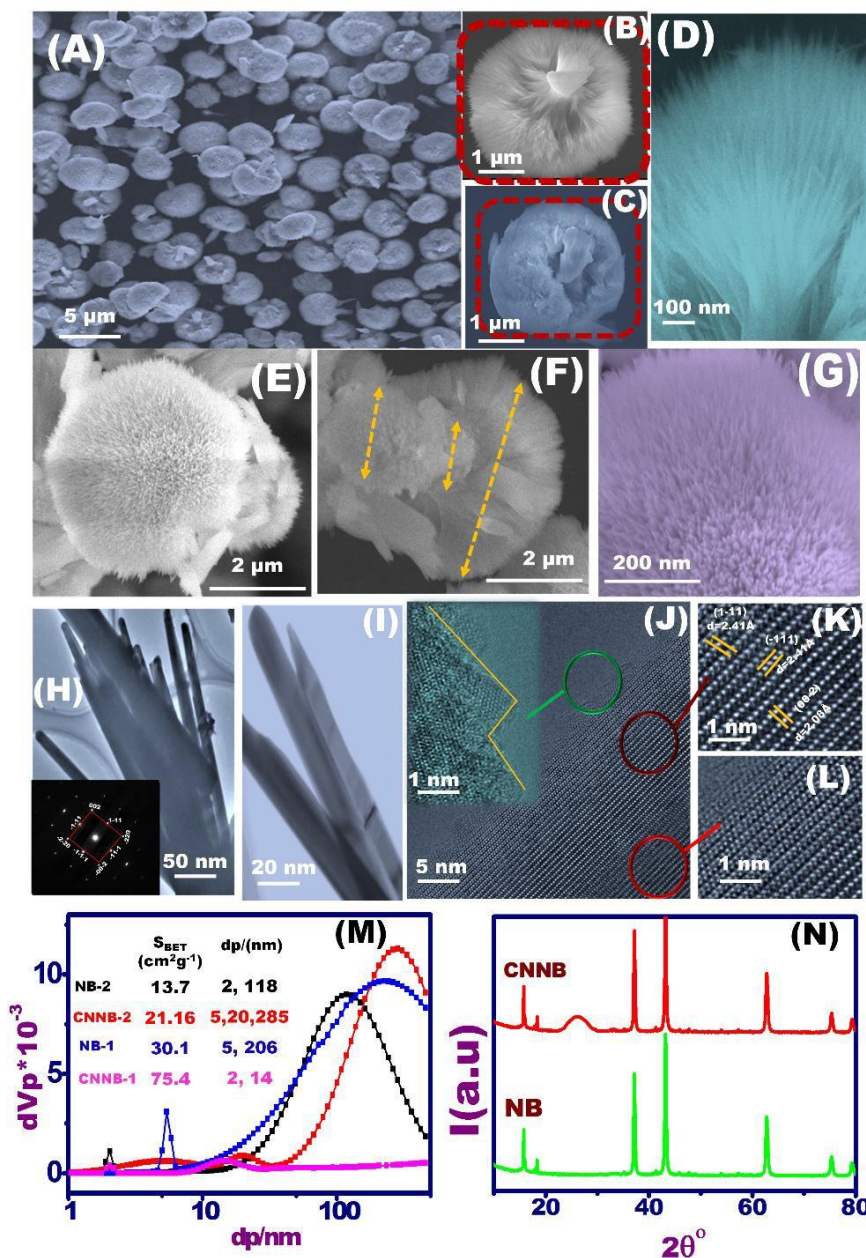


Figure 1. (A) Low magnification of FE-SEM micrograph for CNNB-1. (B) high magnification of FE-SEM for unit construction of NB-1 form vertical back of view, which obtaining the controlled formation of NB unit with head and trunk. (C) high magnification of FE-SEM for NB-1 covered by CN-nanospheres form vertical point of view. (D) HAADF-STEM micrograph focused on the head unit for clearing the surface morphology (E) FE-SEM for NB-2, clearing the difference in head sizes for each unit and confirmed by other unit which clearly represent the size of two different heads and the trunk in-between as in (F). (G) High magnification FE-SEM on the head unit of CNNB-2. (H,I) High magnification of HAADF-STEM focusing on the tubes of the top head surface, inset high-dense ED-STEM, corresponding the atomic configuration along {110} crystal planes. (J) High magnification of HAADF-STEM focusing on the ends of tubes and reflecting the crystalline surface degree, focusing on different degree of the tube at its centre (K), denser for interior head (L) and at its top edge (inset of J).(M) NLDF pore size distribution. (N) XRD patterns of NB and CNNB. Table (inset of M) shows the pore size and S_{BET} for NB-2, NB-1, CNNB-2 and CNNB-1.

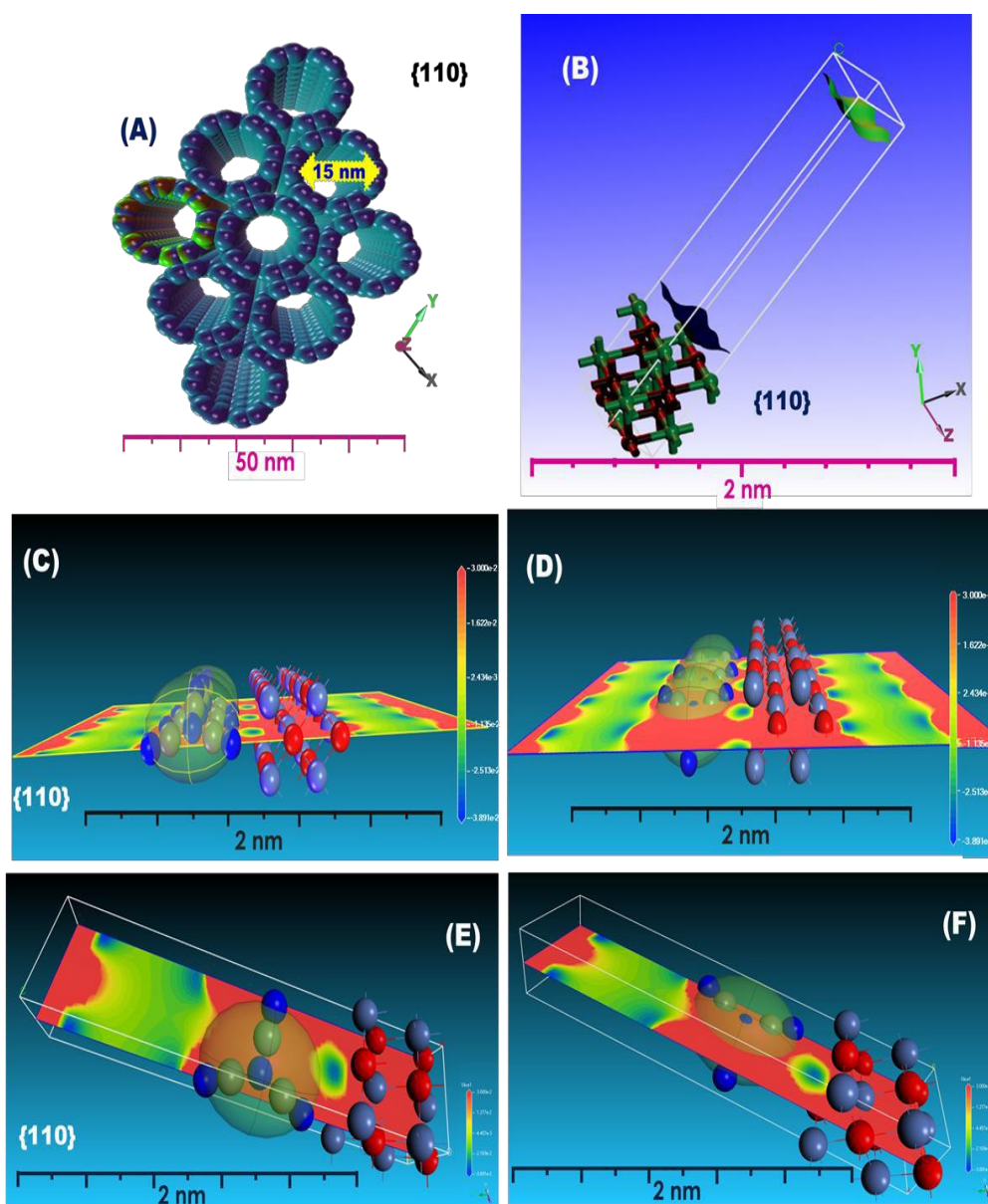


Figure 2. (A) Mesostructured $\{110\}$ -NB crystal facet oriented around the mesopore frameworks. The structure was tilted with 15° . The location of the frame structure along $\{110\}$ plane enabled the actively energetic surface coverage for facile diffusion and strong binding with the target molecules. (B) The atomic organization of NB-1 crystal into exposed $\{110\}$ surface plane. (C, D) High energy surfaces formed along the entire crystal structure directed along $\{110\}$ and $\{101\}$ surface exposure and CN-nanospheres clouds over Ni and O atoms for NB-1 and NB-2, respectively. (E and F) $\{110\}$ and $\{101\}$ -top-surface around double-layer surfaces show high energy electron surfaces formed along the entire NB crystal structure directed along $\{110\}$ and $\{101\}$ surface exposure, particularly at the Ni^{2+} -top surfaces with NC clouds.

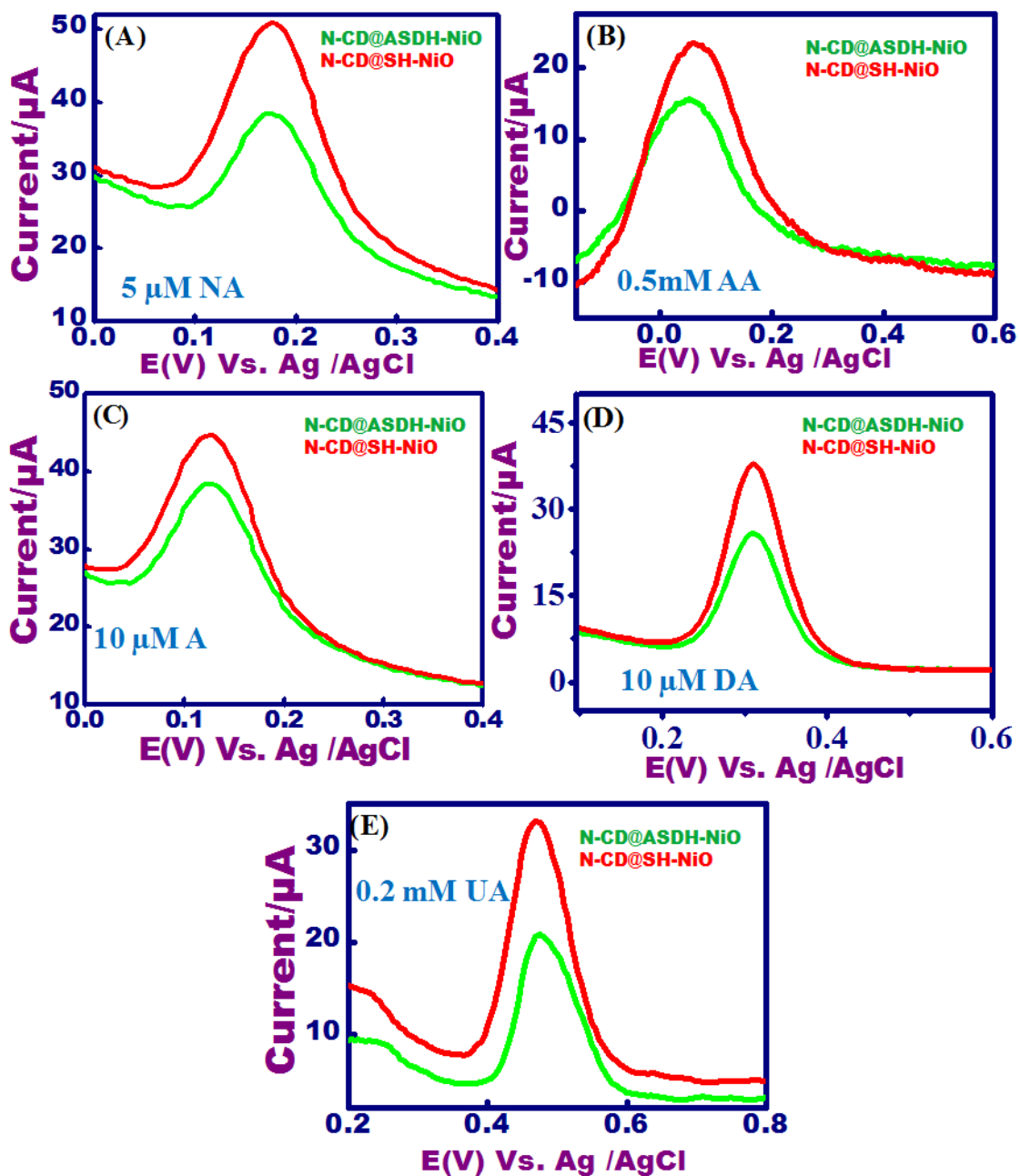


Figure 3. DPV of CNNB-2 (wine line) and CNNB-1 (red line) for 0.2 mM UA (A), 0.5 mM AA (B), 10 μM DA (C) 10 μM A (D) and 5 μM NA (E) in PBS pH= 7 at scan rate = 100 mVs⁻¹, pulse Height = 60 mV, pulse width = 25 ms.

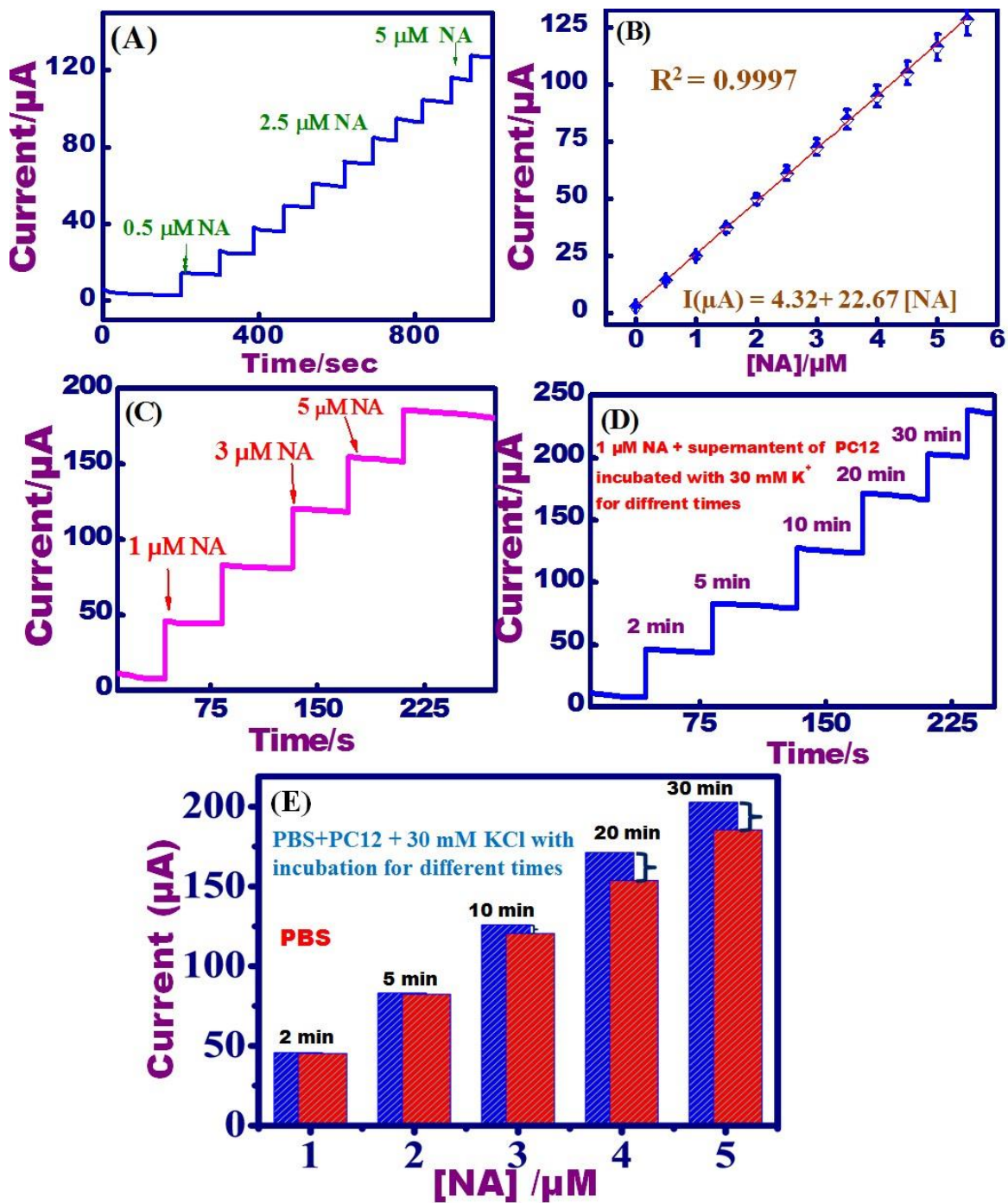


Figure 4. (A) The amperometric response of NA with successive addition from 0.5-5 μM on CNNB-1 nanoelectrode and (B) The linear plot of concentration (μM) Vs the current (μA). (C & D) The amperometric response of NA addition in PBS pH=7 without and with PC12 induced by 30 mM KCl, (E) the column plot of concentration of norarenaline with (blue column) and without (green column) PC12 (30 mM KCl) Vs the current (μA) at applied potential 0.17 V.

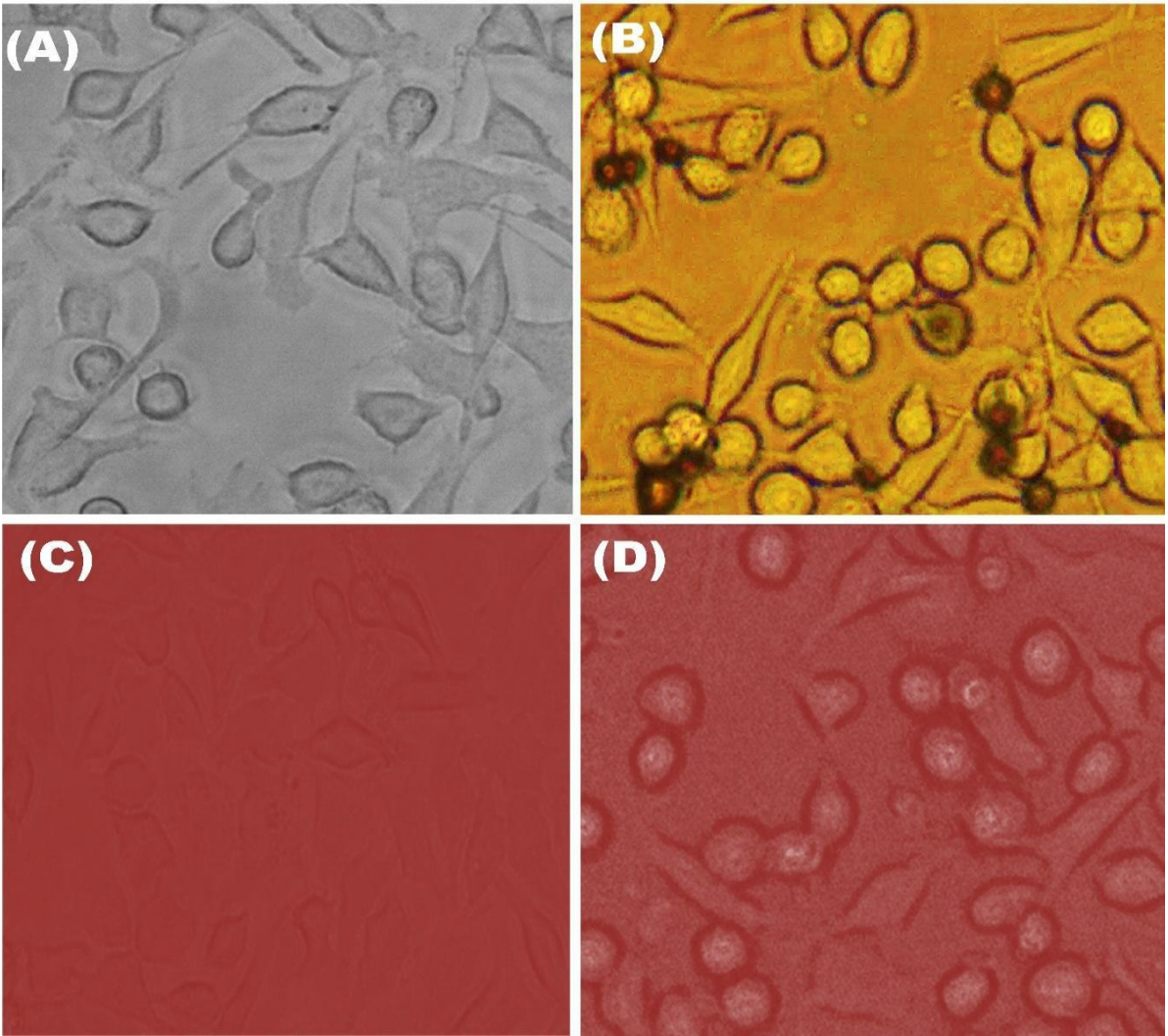


Figure 5. Confocal microscope images recorded at excitation wavelength of 488 nm and emission wavelength at 620 nm of control PC12 cells (A) and incubation of PC12 with 30 mM KCl for 30 min (C), PC12 cells with 20 µg/ml CNNB-1 for 30 min (B) and incubated PC12 +20 µg/ml CNNB-1 with 30 mM KCl for 30 min (D).

Supplementary Material

[Click here to download Supplementary Material: Supporting.docx](#)